Journal of Geophysical Research: Space Physics

RESEARCH ARTICLE
10.1029/2018JA025685

Long-Term Estimation of Diurnal Vertical E × B Drift Velocities Using C/NOFS and Ground-Based Magnetometer Observations

John Bosco Habarulema[1,2], Makhosonke B. Dubazane[1,2], Zama T Katamzi-Joseph[1,2], Endawoke Yizengaw[3], Mark B. Moldwin[4], and Jean Claude Uwamahoro[1,2]

[1]South African National Space Agency, Space Science, Hermanus, South Africa, [2]Department of Physics and Electronics, Rhodes University, Grahamstown, South Africa, [3]Institute for Scientific Research, Boston College, Lexington, MA, USA, [4]Department of Climate and Space Sciences and Engineering, University of Michigan, Ann Arbor, MI, USA

Key Points:
- A relationship between C/NOFS vertical E x B drifts and magnetometer-derived EEJ during 2008-2014 has been developed
- At least 80% of the differences between observed and derived E x B lie within -5 m/s and 5 m/s when validated with radar observations
- The developed relationship is applicable during quiet and disturbed conditions

Correspondence to:
J. B. Habarulema,
jhabarulema@sansa.org.za

Citation:
Habarulema, J. B., Dubazane, M. B., Katamzi-Joseph, Z. T., Yizengaw, E., Moldwin, M. B., & Uwamahoro, J. C. (2018). Long-term estimation of diurnal vertical **E** × **B** drift velocities using C/NOFS and ground-based magnetometer observations. *Journal of Geophysical Research: Space Physics*, *123*, 6996–7010. https://doi.org/10.1029/2018JA025685

Received 21 MAY 2018
Accepted 30 JUL 2018
Accepted article online 6 AUG 2018
Published online 27 AUG 2018

Abstract We report on the development of a new mathematical expression to estimate local daytime (0700–1700 LT) vertical **E**×**B** drift in low latitudes using a combination of ground-based magnetometer measurements and Communications and Navigation Outage Forecasting System (C/NOFS) satellite observations. The expression was developed over Jicamarca (11.8°S, 77.2°W; 0.8°N geomagnetic) and validated with Jicamarca Unattended Long-Term studies of the Ionosphere and Atmosphere (JULIA) mode and incoherent scatter radar (ISR) measurements during the period 2008–2014. The obtained correlation coefficient (*R*) values computed using observed and derived vertical **E** × **B** drift velocities are 0.79 and 0.84 for ISR and JULIA, respectively when data are available during 2008–2014. Storm-time comparison between observed and derived vertical **E** × **B** drift velocities agreed well with *R* of 0.92 and 0.87 during 5–8 August 2011 and 8–11 March 2012 geomagnetic storm periods for ISR and JULIA observations, respectively. Overall, we found that the developed expression is applicable in estimating vertical **E** × **B** drift response during quiet and geomagnetic storm periods. Based on these findings, we suggest that it is possible to develop accurate daytime global vertical **E** × **B** drift model over the equatorial latitude regions using inexpensive magnetometer observations and available satellite data.

1. Introduction

The importance of zonal electric fields in influencing plasma electrodynamics in low or equatorial latitude regions is well known (e.g., Fejer et al., 2008; Huang et al., 2005; Patra et al., 2004, 2014; Scherliess & Fejer, 1997; 1999) and includes controlling the extent of the equatorial ionization anomaly and vertical coupling between the low- and high-altitude ionospheric layers and associated physical processes. However, in general, electric field data remain sparse in most longitude sectors. Traditionally, day-to-day variability studies of equatorial vertical **E** × **B** drifts at all local times were possible using the Jicamarca incoherent scatter radar (ISR). The evidence that 150-km echoes are a proxy of *F*2 region vertical **E** × **B** drifts (e.g.,Chau & Woodman, 2004; Kudeki & Fawcett, 1993) has made it possible to study changes of vertical **E** × **B** drifts in other longitude sectors during local daytime (Patra & Rao, 2006; Patra et al., 2008). Although there have been deployment of backscatter 150-km echo radars that have filled data gaps in different longitude sectors such as India and Indonesia (Patra & Rao, 2006; Patra et al., 2008, 2012, 2014), there is still limited vertical **E** × **B** drift observations in other regions hindering accurate understanding of the global ionospheric plasma dynamics. It therefore still remains necessary to explore different techniques or approaches that can improve data coverage both in time resolution domain and in different longitude sectors. In this regard, satellite data provide the necessary global coverage, but are noncontinuous over particular longitude sectors and local times and are hence more appropriate for developing climatological models. Logistically, it is almost impossible to deploy radars at all longitude sectors due to the huge acquisition and operational costs. In an effort to increase continuous vertical **E** × **B** drift data coverage in low/equatorial latitudes, we propose a simple mathematical approach based on simultaneous consideration of ground-based magnetometer and Communications and Navigation Outage Forecasting System (C/NOFS) satellite data. The first challenge with this is how to validate the proposed approach since vertical **E** × **B** drift data are scarce in many longitude sectors. For the beginning, this is best done over a location or longitude sector with extended vertical **E** × **B** drift observational data, which makes

Jicamarca (11.8°S, 77.2°W; 0.8°N geomagnetic) an excellent choice for this study. The developed approach can then be transferable to other longitude sectors with a particular level of confidence. We have developed a simple expression relating daytime equatorial electrojet (EEJ) estimated from magnetometer measurements (ΔH) using the differential method (e.g., Anderson et al., 2002, 2004; Rastogi & Klobuchar, 1990) and C/NOFS vertical component of the ion plasma drift observations over Jicamarca during 2008–2014. These two data sets can be related based on previous findings that ground-based magnetometer derived EEJ approximates daytime changes in the vertical component of the phase velocity of irregularities near 150 km (e.g., Anderson et al., 2004; Chau & Woodman, 2004) which correspond to the vertical ion drift and thus the zonal electric field in equatorial regions. The developed expression was validated with Jicamarca ISR's vertical $\mathbf{E}\times\mathbf{B}$ drift and Jicamarca Unattended Long-term studies of the Ionosphere and Atmosphere (JULIA) system data, including separate treatment of different geophysical conditions. We wish to state that it has been shown previously that JULIA vertical $\mathbf{E}\times\mathbf{B}$ drift data correlate well with EEJ (e.g., Anderson et al., 2004) and have high agreement with ISR vertical $\mathbf{E}\times\mathbf{B}$ drift observations (Chau & Woodman, 2004; Kudeki & Fawcett, 1993). A clear historical perspective linking 150-km echo Doppler velocities to equatorial vertical drifts along with relevant references has been presented in Rodrigues et al. (2015). Ground-based magnetometer data have advantage of being continuous with high temporal resolution and are available in a number of longitude sectors, thus increasing the probability of getting coincidental observations when the satellite is within the vicinity of the magnetometer location. It is established that the difference between horizontal components of the Earth's magnetic field observations (ΔH) from magnetometer locations at the equator and about 6° – 9° away from the equator is a proxy of EEJ, which has a linear relationship with vertical $\mathbf{E}\times\mathbf{B}$ drift (Anderson et al., 2002, 2004; Yizengaw et al., 2014) during local daytime. Therefore, the development of a mathematical relationship between C/NOFS vertical ion plasma drift and ΔH has the potential to provide high temporal resolution vertical $\mathbf{E}\times\mathbf{B}$ databases in longitude sectors where low-latitude magnetometers exist. This would in turn contribute to formulation of empirical models in equatorial latitudes as well as performing extended day-to-day vertical drift variability on a long-term basis by utilizing the extended magnetometer network consisting of pairs that satisfy the criteria for estimating EEJ (e.g., Yizengaw & Moldwin, 2009). Although the approach based on magnetometer observations is valid during local daytime, it may be possible in future to develop $\mathbf{E}\times\mathbf{B}$ drift models covering all times by combining vertical $\mathbf{E}\times\mathbf{B}$ drift data estimated from daytime magnetometer ΔH and nighttime satellite observations.

2. Data Sources and Method

The Ion Velocity Meter, one of the instruments of the Coupled Ion Neutral Dynamics Investigation package on board C/NOFS satellite provides in situ observations of equatorial meridional/vertical component of the ion plasma drift (e.g., Stoneback et al., 2011, 2012; Yizengaw et al., 2014) that are used in this study. C/NOFS satellite which was launched in April 2008 in a 13° inclination orbit had initial perigee and apogee at 400 km and 850 km, respectively (Stoneback et al., 2011). The Ion Velocity Meter instrument provides vertical ion plasma drift, ion composition, and temperature. Detailed information about the instrument calibration for ion plasma drift measurements can be found in Stoneback et al. (2012). The other instrument of Coupled Ion Neutral Dynamics Investigation is the neutral wind meter that gives neutral velocity and density observations. In our analysis, we limited C/NOFS vertical ion plasma drift (equivalent to vertical $\mathbf{E}\times\mathbf{B}$ drift at about 400 km) observations within ±4° latitude from the geomagnetic equator based on the fact that the EEJ is a strip of enhanced current within ±3° from the dip equator. Also, a study by Manoj et al. (2006) showed that the correlation between EEJ derived from ground-based magnetometer data and CHAMP satellite observations deteoriated beyond ±4° from the geomagnetic equator. The longitudinal consideration was limited within 77.2°W ± 8° to ensure that the local time did not change considerably, while the altitude range was 400–550 km, which has been used in several investigations (e.g., Rodrigues et al., 2015; Stoneback et al., 2011; Yizengaw et al., 2014). From now onward and for convenience purposes, there may be instances where C/NOFS vertical ion plasma drift is simply referred to as C/NOFS vertical $\mathbf{E}\times\mathbf{B}$ drift, especially during the comparison with ISR and JULIA measurements. The outliers in C/NOFS vertical $\mathbf{E}\times\mathbf{B}$ data were removed per satellite pass (within our defined latitude/longitude and altitude grid) using the median filtering technique centered at determining the median and median absolute deviation. The scaled median deviation (δ) was determined following a procedure in Huber (1981), Huber and Ronchetti (2009), and Lomidze et al. (2018) as $\delta = b \times \text{median}(|y_i - \text{median}(y_i)|)$, where the constant $b = 1.4826$ is associated with data exhibiting normal distribution (e.g., Leys et al., 2013; Rousseeuw & Croux, 1993) and y_i are the time series observations, in

this case, per satellite pass within the defined spatial/altitude resolution. Therefore, values outside the range; median $\pm$ 2.5δ (per satellite pass) were eliminated from further analysis. In total, the combination of median and scaled median absolute deviation removed 2.82% of C/NOFS vertical ion drift as outliers which did not exhibit regular trend in their diurnal temporal variability.

The EEJ was determined from horizontal component of the Earth's magnetic field using a pair of magnetometer stations; Jicamarca (11.8°S, 77.2°W; 0.8°N geomagnetic) and Piura (5.2°S, 80.6°W; 6.8°N geomagnetic). Differencing *H* component (to give ΔH) using magnetometer data from a station located at the equator and another one away from the equator by 6°–9° is a widely accepted method of determining EEJ and or vertical $\mathbf{E}\times\mathbf{B}$ drift (Anderson et al., 2002, 2004; Rastogi & Klobuchar, 1990; Yizengaw et al., 2011, 2012) during local daytime. The reader is referred to Anderson et al. (2002, 2004) and Yizengaw et al. (2012) for a detailed description of the method.

Figure 1 shows (a) the location of Jicamarca and Piura magnetometer stations (red dots) along with the spatial coverage considered for C/NOFS vertical ion drifts (enclosed in blue dashed lines) around Jicamarca, (b) daytime *H* (nT) after removing the background *H* value by subtracting the average nighttime baseline value between 2300 and 0300 local time (Yizengaw et al., 2014) over Jicamarca (black curve) and Piura (blue curve) for 8 January 2011, and (c) daytime ΔH (nT) obtained using data in (b) as well as available C/NOFS vertical ion drift (m/s) (plotted as black dots) on 8 January 2011. Figure 1c shows that for most of the time when data are available, C/NOFS vertical ion plasma drift and magnetometer ΔH agree even in revealing downward vertical drifts manifesting as negative values in the observations. There were considerable instances with negative values of ΔH and C/NOFS vertical ion drift during our period of study as we will show later in the next section. It has long been established that counterelectrojet (CEJ) occurs during local daytime in low solar activity conditions (Rastogi, 1974). A recent longitudinal study over the African, South American, and Phillipine regions during 2009 showed that there were occurrences of CEJ sometimes in local morning and especially in later afternoon (Rabiu et al., 2017). Some of the mechanisms associated with CEJ include vertical upward winds in equatorial regions (e.g., Raghavarao & Anandarao, 1980) and Sudden Stratospheric Warming (SSW) driven dynamo processes (Vineeth et al., 2009). As a result of the prolonged solar minimum that caused complexities in ionospheric changes especially during 2008–2011 (Chen et al., 2011; Perna & Pezzopane, 2016), our subsequent analysis and statistics involve significant CEJ durations when ΔH and C/NOFS vertical ion plasma drifts were negative.

3. Relationship Between C/NOFS Vertical Ion Plasma Drift and Magnetometer Observations

Selecting C/NOFS vertical ion plasma (or simply vertical $\mathbf{E}\times\mathbf{B}$) drift data and ΔH at times when both data sets are available within 2008–2014 yields a data set that can be used to develop a mathematical relationship between these two variables. The exact data range used starts from 5 September 2008 (at 1206 LT) to 6 March 2014 (1005 LT). Figure 2 shows the outcome of C/NOFS vertical ion plasma drift and ΔH data with a correlation coefficient of 0.57 (number of data points is 3,939) during local daytime (0700–1700 LT). Recently, Kumar et al. (2016) reported similar results by comparing EEJ and vertical $\mathbf{E}\times\mathbf{B}$ drifts from ROCSAT-1 in the Indian and Japanese sectors and over Jicamarca where a simultaneous comparison was done using JULIA and EEJ to assess the agreement at different altitudes. Using data during 2001–2013, Kumar et al. (2016) obtained correlation coefficient values of 0.61 and 0.56 between ROCSAT measurements and ΔH over the Indian and Japanese sectors, respectively. When separated according to levels of geomagnetic activity, correlation values during quiet conditions ($Kp < 3$) were 0.6 and 0.52 over the Indian and Japanese sectors, respectively, during 2001–2003. It therefore appears that correlation values do not vary much based on geophysical conditions. Magnetometer data have temporal resolution of 1 min and were used as a benchmark for choosing the coincidental C/NOFS data. A relationship between JULIA vertical $\mathbf{E}\times\mathbf{B}$ drifts and magnetometer ΔH has previously been established (Anderson et al., 2004) over Jicamarca using 2001–2003 data sets. Among the different approaches investigated, Anderson et al. (2004) developed an expression estimating vertical $\mathbf{E}\times\mathbf{B}$ drifts as a third-order polynomial function of ΔH using JULIA and magnetometer measurements during local daytime. We note that this expression was developed for data sets that were close in terms of altitude variations. Magnetometer ΔH is a proxy of EEJ which is the eastward current within the ionospheric *E* region at ≃120 km (Anderson et al., 2004; Rastogi & Klobuchar, 1990; Richmond, 1973), while JULIA vertical $\mathbf{E}\times\mathbf{B}$ drift data are regarded as measurements at 150 km (e.g., Chau & Woodman, 2004; Kudeki & Fawcett, 1993;

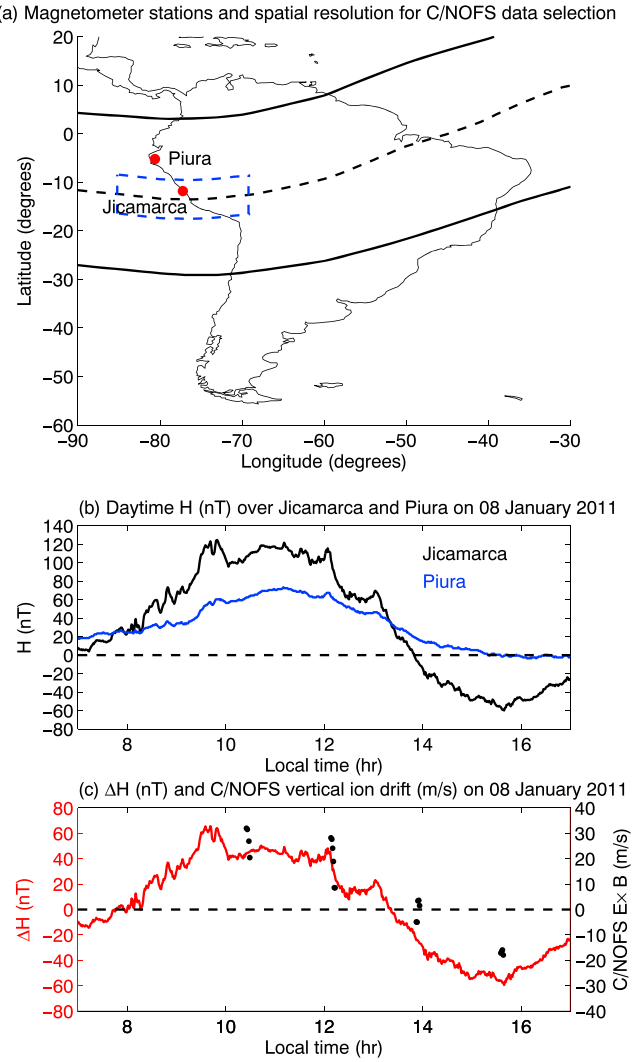

Figure 1. (a) Location of magnetometer stations (red dots), illustration of the spatial coverage (within the blue enclosure) used for C/NOFS vertical ion drift data consideration within altitude of 400–550 km around Jicamarca, (b) daytime *H* (nT) after removing the background *H* value by subtracting the average nighttime baseline value between 2300 and 0300 local time over Jicamarca (black curve) and Piura (blue curve) for 8 January 2011, and (c) daytime ΔH (nT) or simply EEJ obtained using data in (b) along with available C/NOFS vertical ion drift (m/s) (plotted as black dots) on 8 January 2011. In (a), the dashed black line represents the geomagnetic equator while the solid black lines show the southern and northern crests of the equatorial ionization anomaly at ±15° from the geomagnetic equator. C/NOFS = Communications and Navigation Outage Forecasting System.

Patra et al., 2014). In our case, we are correlating ΔH (EEJ) at ≃120 km with C/NOFS vertical ion plasma drift (altitude range of 400–550 km) and therefore should experimentally determine the appropriate mathematical function that best relates the two sets of measurements. To determine the solution, we tested a number of functions relating C/NOFS vertical ion plasma drift and ΔH (in Figure 2) and estimated vertical $\mathbf{E}\times\mathbf{B}$ drift for the entire ΔH database during times when the ISR made observations (over the period 2008–2014). The ISR observations were later used to validate the performance of each investigated expression. Table 1 shows the root-mean-square error, RMSE (m/s) and correlation coefficient (*R*) values for the different functions investigated.

In Table 1, statistical values indicate that vertical $\mathbf{E}\times\mathbf{B}$ is best estimated with a cubic function of ΔH, which has the lowest RMSE (7.13 m/s) and high *R* (0.78) over the interval 2008–2014. We suggest that this method can be adopted for other longitude sectors (since satellite data are available) where there are magnetometer measurements, hence increasing day-to-day vertical $\mathbf{E}\times\mathbf{B}$ drift coverage that has been previously limited to

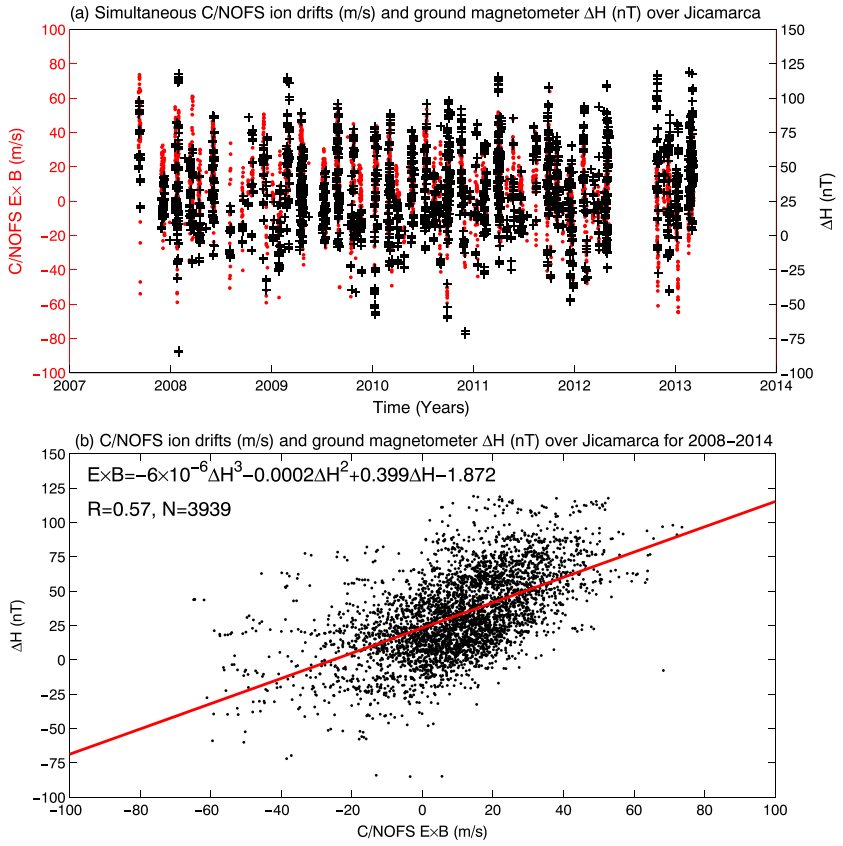

Figure 2. Representation of (a) simultaneous C/NOFS vertical ion plasma drifts (red dots) equivalent to vertical $\mathbf{E}\times\mathbf{B}$ drift (m/s) and ΔH (nT; black positive sign) availability (2008–2014) over Jicamarca during local daytime (0700–1700 LT); and (b) scatter plot of C/NOFS vertical ion plasma drift or $\mathbf{E}\times\mathbf{B}$ drift (m/s) and ΔH (nT). The derived cubic expression is shown in (b) along with correlation coefficient (*R*) of 0.57 obtained using 3,939 number of observations. C/NOFS = Communications and Navigation Outage Forecasting System.

regions with radar instrumentation. However, the coefficients of the cubic function should be redetermined for each longitude sector under consideration to take into account local time effects such as contributions to vertical $\mathbf{E}\times\mathbf{B}$ drifts arising from *E* region migrating and nonmigrating tides and longitudinal conductivity differences (Lühr et al., 2008; Millward et al., 2001). A vital aspect to mention is that our study included the extended low solar activity period of 2008–2010 where low correlation between solar activity and vertical drift has been reported over the African sector (Dubazane et al., 2018). Observations during the extended solar minimum of 2008–2009 showed complex behavior as they disagreed with the previously established understanding that vertical $\mathbf{E}\times\mathbf{B}$ drifts have solar activity dependance (e.g.,Fejer et al., 1991; Richmond, 1973) over the equatorial latitudes. Figure 3a shows the JULIA vertical $\mathbf{E}\times\mathbf{B}$ drift variability from 2001 to 2015 at 1200 LT. The solar flux F10.7 is superimposed on Figure 3a and generally shows little correlation from 2008

Table 1
RMSE and Correlation Coefficient (R) Values Between Vertical $\mathbf{E}\times\mathbf{B}$ *Drift Estimated From the C/NOFS Vertical Ion Plasma Drift-Magnetometer ΔH Relationship and Available ISR Measurements Over Jicamarca During 2008–2014*

Function of ΔH for $\mathbf{E}\times\mathbf{B}$ estimation	Correlation coefficient (*R*)	RMSE (m/s)
Linear	0.762	7.27
Quadratic	0.774	7.309
Cubic	0.777	7.134
Fourth-order polynomial	0.774	7.198
Fifth-order polynomial	0.756	7.437

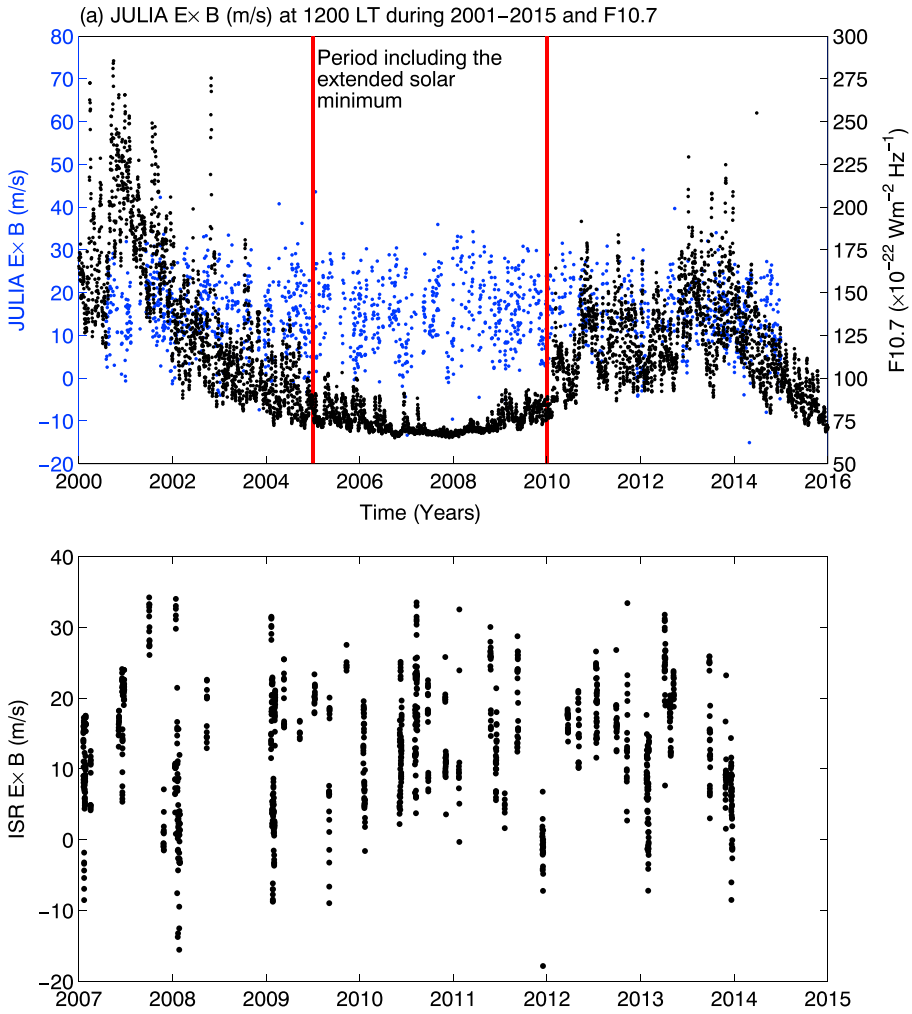

Figure 3. (a) Comparison of JULIA vertical $\mathbf{E}\times\mathbf{B}$ (m/s) variability at 1200 LT (2001–2015) with solar flux at 10.7 cm wavelength, F10.7 (2000–2016). The vertical red lines highlight the period (2005–2010) including the prolonged solar minimum. Panel (b) shows an example of ISR $\mathbf{E}\times\mathbf{B}$ (m/s) availability at 1200 LT from 2008 to 2014 used in evaluating the derived expression between C/NOFS vertical ion drifts and ground-based magnetometer ΔH (nT). JULIA = Jicamarca Unattended Long-Term studies of the Ionosphere and Atmosphere; C/NOFS = Communications and Navigation Outage Forecasting System.

to 2010, which may be directly related to the complexity of the ionospheric variability during this extended solar minimum period (Chen et al., 2011; Ezquer et al., 2014; Perna & Pezzopane, 2016; Solomon et al., 2013). In Figure 3b ISR vertical $\mathbf{E}\times\mathbf{B}$ drift changes are shown at 1200 LT during 2008–2014. Figure 3 generally demonstrates that JULIA data are more extensive than ISR data during our period of study, 2008–2014. Based on the data presented in Figure 3a showing no clear correlation between vertical $\mathbf{E}\times\mathbf{B}$ drift velocities and solar activity during the extended solar minimum, we have also investigated developing separate expressions for estimating vertical $\mathbf{E}\times\mathbf{B}$ drift in 2008–2010 and 2011–2014; and compared results with the combined data sets' outputs. The final expressions are

$$\mathrm{E}\times\mathrm{B} = -6\times10^{-6}\Delta H^3 - 0.0002\Delta H^2 + 0.399\Delta H - 1.872, \text{for } 2008-2014 \quad (1)$$

$$\mathrm{E}\times\mathrm{B} = -3\times10^{-5}\Delta H^3 + 0.002\Delta H^2 + 0.484\Delta H + 0.123, \text{for } 2008-2010 \quad (2)$$

$$\mathrm{E}\times\mathrm{B} = 7\times10^{-6}\Delta H^3 - 0.001\Delta H^2 + 0.361\Delta H - 3.488, \text{for } 2011-2014 \quad (3)$$

Equations (1)–(3) were developed from the C/NOFS vertical ion plasma drift and ground-based magnetometer derived ΔH presented in Figure 2. The next section presents validation results of the developed expressions.

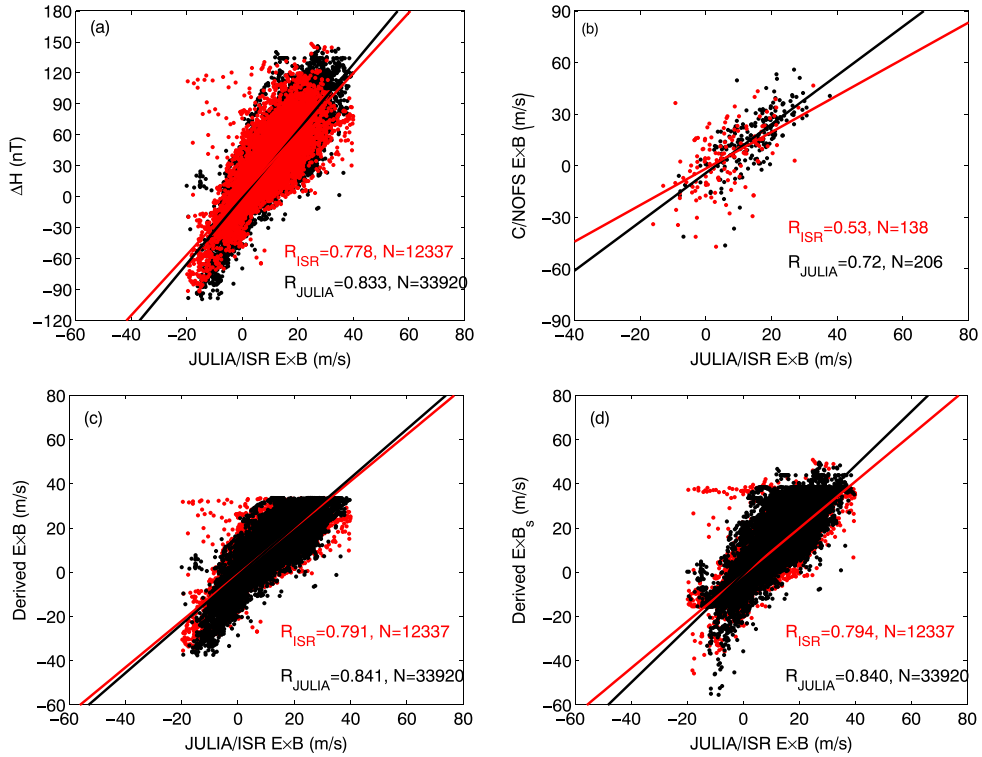

Figure 4. Scatter plots of measured (JULIA and ISR) vertical $\mathbf{E}\times\mathbf{B}$ drift and (a) ΔH, (b) C/NOFS vertical $\mathbf{E}\times\mathbf{B}$, (c) derived vertical $\mathbf{E}\times\mathbf{B}$ drift using equations (1), (d) derived vertical $\mathbf{E}\times\mathbf{B}$ drift using equations (2) and (3). JULIA = Jicamarca Unattended Long-Term studies of the Ionosphere and Atmosphere; ISR = incoherent scatter radar; C/NOFS = Communications and Navigation Outage Forecasting System.

4. Results and Discussion

Figure 4 shows scatter plots of observed (JULIA and ISR) vertical $\mathbf{E}\times\mathbf{B}$ drift and (a) ΔH, (b) C/NOFS vertical $\mathbf{E}\times\mathbf{B}$ drift, (c) derived $\mathbf{E}\times\mathbf{B}$ drift using equation (1), and (d) derived $\mathbf{E}\times\mathbf{B}$ drift using equations (2) and (3). The JULIA mode of the Jicamarca ISR provides *E* region (~150 km) vertical irregularity drift assumed to be almost equivalent to the background vertical $\mathbf{E}\times\mathbf{B}$ drift as shown in literature (e.g., Chau & Woodman, 2004). The ISR provides drift profiles (200–800 km) and this study used the publicly available averaged drifts in the range 225–600 km. We should add that restricting ISR altitudes within the C/NOFS altitude (400–550 km) data consideration did not significantly change results. In Figure 4a, the correlation between ΔH and JULIA vertical $\mathbf{E}\times\mathbf{B}$ drift is higher (0.833) than the corresponding value for ISR vertical $\mathbf{E}\times\mathbf{B}$ drift (0.778). When ISR altitude averaging was limited to 400–550 km, the correlation coefficient value slightly changed to 0.75. The difference in correlation values between ΔH and JULIA/ISR vertical drifts is expected due to the altitudinal difference at which JULIA and ISR provide $\mathbf{E}\times\mathbf{B}$ measurements. While JULIA vertical $\mathbf{E}\times\mathbf{B}$ drift data (at lower bottomside *F*2 region of 150-km altitude) can be regarded as observations at constant altitude, it has been demonstrated that ISR vertical $\mathbf{E}\times\mathbf{B}$ drifts have temporal altitudinal variability exhibiting a general increase and decrease with altitude during morning and afternoon hours, respectively (e.g., Hui & Fejer, 2015; Pingree & Fejer, 1987). Correlation results in Figure 4b for the case of JULIA and C/NOFS vertical $\mathbf{E}\times\mathbf{B}$ give $R_{\mathrm{JULIA}} = 0.72$ compared to $R_{\mathrm{ISR}} = 0.53$ for ISR and C/NOFS vertical $\mathbf{E}\times\mathbf{B}$. Due to the altitude consideration, one would expect the correlation to be higher for C/NOFS and ISR vertical drifts. It is noted that there were less cases of coincidental C/NOFS and ISR vertical drifts observations, making it a bit difficult to conclude based on limited information. Relatively low correlation between C/NOFS vertical $\mathbf{E}\times\mathbf{B}$ drift and JULIA/ISR measurements (compared to *R* values for ΔH and ISR/JULIA data) is partly attributed to the different physical mechanisms at different altitudes, and the fact that a longitudinal range of 16° for C/NOFS vertical $\mathbf{E}\times\mathbf{B}$ drift is considered.

In terms of correlation with respect to local time dependance, Table 2 shows *R* values computed between ΔH and C/NOFS vertical ion plasma drift and derived and observed ISR/JULIA $\mathbf{E}\times\mathbf{B}$ drift during 2008–2014 at different times with interval of 2 hr. While the *R* values between ΔH and C/NOFS vertical ion plasma drift

Table 2
Correlation Coefficient Values for Different Local Time Ranges During 2008–2014 Over Jicamarca

	Correlation coefficient (*R*) between		
Local time range	ΔH (nT) and C/NOFS vertical ion drift (m/s)	Derived and observed ISR **E** × **B** (m/s)	Derived and observed JULIA **E** × **B** (m/s)
07:00–09:00	0.558	0.802	0.820
09:00–11:00	0.583	0.705	0.868
11:00–13:00	0.524	0.766	0.847
13:00–15:00	0.385	0.833	0.818
15:00–17:00	0.230	0.803	0.737

Note. C/NOFS = Communications and Navigation Outage Forecasting System; JULIA = Jicamarca Unattended Long-Term studies of the Ionosphere and Atmosphere; ISR = incoherent scatter radar.

are significantly lower for 13:00–15:00 LT and 15:00–17:00 LT, we see higher (above 0.7) *R* values between derived and observed ISR/JULIA **E** × **B** drift at all local times. Starting from the developed expression relating ΔH and C/NOFS vertical ion plasma drift; which was later used to derive both ISR and JULIA vertical **E** × **B** drift at times when their observations were available, we notice that the primary trend determinant of the derived vertical **E** × **B** drift values is ΔH. Therefore, if the trend behavior of vertical drift variability is captured in ΔH changes (which is usually the case), we expect improved results of derived ISR/JULIA vertical **E** × **B** drift. In this case, the coefficients will affect mainly the magnitude and not the trend of the derived values. The *R* values between ΔH and C/NOFS vertical ion plasma drift, derived and observed ISR vertical **E** × **B** drift, and derived and observed JULIA vertical **E** × **B** drift are 0.534, 0.766, and 0.846, respectively, during 1000–1400 LT. The general high correlation between derived and observed JULIA vertical **E** × **B** drift could be due to the fact that the altitudinal difference between the EEJ (ΔH) and JULIA observations is relatively small (about 40 km) compared to the range of ISR or C/NOFS observations. Additionally, afternoon downward drifts observed in C/NOFS data have been reported (Stoneback et al., 2011), which were found to be absent in JULIA 150-km echo drifts (Rodrigues et al., 2015). This is partly responsible for the lower *R* values reported in Table 2 during 13:00–17:00 LT as the downward drifts seen in C/NOFS vertical ion plasma drift could be absent in ΔH. Overall, during 1300–1500 LT and 1500–1700 LT, simultaneous occurrence of negative C/NOFS vertical ion plasma drift and ΔH accounted for 5.99% and 5.56%, respectively. For the 1300–1500 LT range, negative values of C/NOFS vertical ion plasma drift made up 31% in comparison with 11% for ΔH. These values slightly changed to 36% and 10% for C/NOFS vertical ion plasma drift and ΔH, respectively, during 1500–1700 LT. Figure 4b was generated by limiting C/NOFS vertical **E** × **B** drift observations within ±4° latitude and 77.2°W ± 8° geographic longitude around Jicamarca. Previous studies have used an extended latitude of about 8°–10° away from the geomagnetic equator (e.g.,Patra et al., 2014; Stoneback et al., 2011; Yizengaw et al., 2014) and obtained high correlation values with 150-km echo radar measurements (e.g.,Patra et al., 2014). However, for the development of the relationship involving EEJ-derived data that is applicable over an extended period covering different solar activity levels, it is necessary to limit the latitude range to within the EEJ region in our analysis. Using the developed relationship in equation (1) (that comprised data in Figure 2 from 2008 to 2014) to derive vertical **E** × **B** drift during periods when the ISR and JULIA made measurements, the scatter plot between derived and observed values is shown in Figure 4c. It is observed that there is a slight improvement in the correlation for ISR and JULIA observations with *R* values of 0.791 and 0.841, respectively, when compared with ΔH (Figure 4a). Previously, Anderson et al. (2004) developed the same order of polynomial function of ΔH based on JULIA vertical **E** × **B** drift. Interestingly, a direct comparison (not shown) with Anderson et al. (2004) expression gives *R* values of 0.76 and 0.83 for ISR and JULIA vertical **E** × **B** drift, respectively, during 2008–2014. Considering expressions developed separately for low (2008–2010) and high (2011–2014) solar activity periods (using expressions in equations (2) and (3) due to the extended nature of the deep solar minimum, the results are shown in Figure 4d for derived vertical drift denoted as $\mathbf{E} \times \mathbf{B}_s$ and observations from JULIA and ISR. The accuracy is almost the same, and so the development of separate expressions seems not to significantly change results. This agrees with the study of Rodrigues et al. (2015), which found that the extreme solar minimum during 2008–2009 did not lead to noticeable changes/effects in daytime JULIA vertical **E** × **B** drifts. We, however, think that if *F*10.7 or any solar activity indicator was used as an input, the results would perhaps be different and so it is advantageous to use ΔH that seems to exhibit the inherent behavior of **E** × **B** changes.

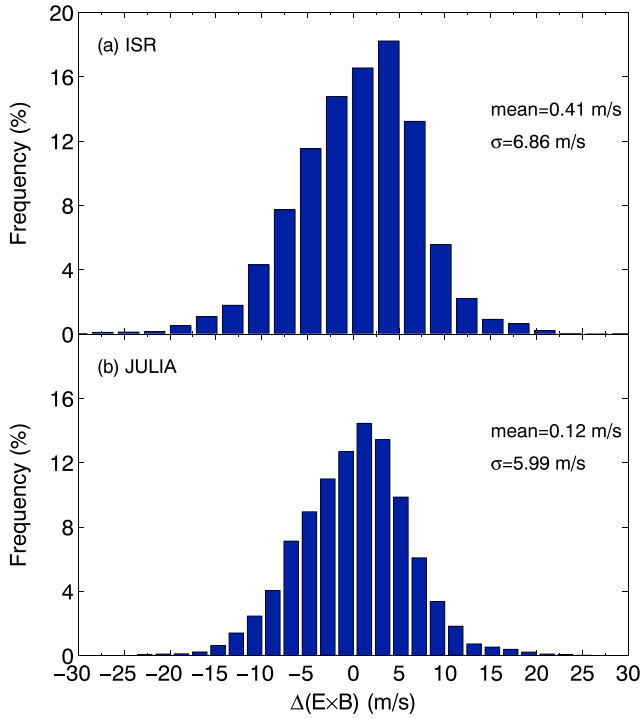

Figure 5. Distribution of differences (observed-derived = $\Delta(\mathbf{E}\times\mathbf{B})$) between derived and observed (a) ISR, and (b)JULIA vertical $\mathbf{E}\times\mathbf{B}$ drifts during for 2008–2014. ISR = incoherent scatter radar; JULIA = Jicamarca Unattended Long-Term studies of the Ionosphere and Atmosphere.

From now onward, the discussion will only use derived vertical $\mathbf{E}\times\mathbf{B}$ drifts using equation (1) that contains coefficients from the entire data set (2008–2014) used in our study.

Figure 5 shows the distribution of the differences (observed-derived) between the derived and observed vertical $\mathbf{E}\times\mathbf{B}$ drift velocities for (a) ISR and (b) JULIA in 2008–2004. In both cases, the mean differences are close to 0 m/s and the standard deviation values are basically the same. For both ISR and JULIA vertical $\mathbf{E}\times\mathbf{B}$ observations, at least 80% of differences lie within −5 m/s and 5 m/s when the developed relationship is validated over the entire available respective data sets during 2008–2014. We have investigated the potential of the developed expression in estimating local daytime vertical $\mathbf{E}\times\mathbf{B}$ response during geomagnetic storms. For this purpose, we considered strong geomagnetic storms with $Dst \leq -100$ nT during 2008–2016 when ISR and JULIA observations were simultaneously available with ΔH measurements. Table 3 shows the summary of correlation coefficient and RMSE values for different storm periods with $Dst \leq -100$ nT during 2008–2016 when we had ΔH and vertical drift data over Jicamarca. There were only two storm periods when ISR vertical drifts and ΔH were present. Important to point out is that Table 3 contains results of 2015 and 2016 which

Table 3
Summary of Correlation Coefficient and RMSE Values for Different Storm Periods With $Dst \leq -100$ nT during 2008–2016 When ΔH and Vertical Drift Data Were Simultaneously Available Over Jicamarca

Storm period	Minimum *Dst* (nT)	*R*	RMSE (m/s)	Data source
5–8 August 2011	−107	0.92	4.37	ISR
8–11 March 2012	−131	0.87	4.31	JULIA
8–10 October 2012	−105	0.77	7.06	JULIA (only 8 Oct had data)
13–15 November 2012	−108	0.96	3.88	JULIA (only 14 Oct had data)
25–27 August 2015	−100	0.78	5.08	ISR
7–8 October 2015	−124	0.80	5.99	JULIA
19–21 January 2016	−104	0.92	4.99	JULIA (19 and 20 Oct had data)

Note. RMSE = root-mean-square error.

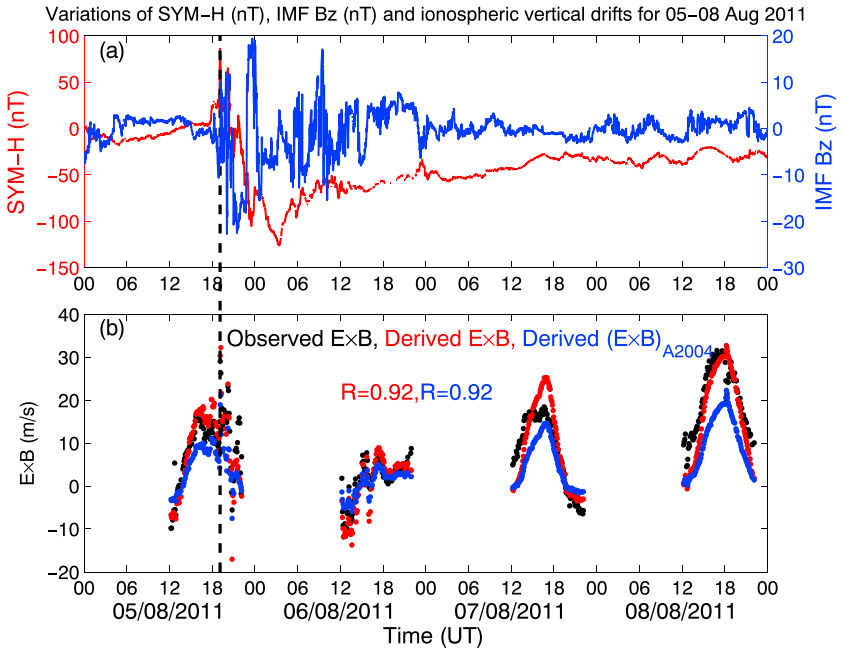

Figure 6. Changes in (a) SYM-H (nT) and IMF Bz (nT) for 5–8 August 2011 storm period, (b) ISR-observed (black dots) and ISR-derived vertical $\mathbf{E}\times\mathbf{B}$ (m/s) with C/NOFS (red dots) and JULIA (blue dots denoted as $(\mathbf{E}\times\mathbf{B})_{\mathbf{A2004}}$ obtained using expression developed by Anderson et al., 2004) based functions during the storm period of 5–8 August 2011. The vertical dashed line represents the storm onset time at 1906 UT on 5 August 2011. Jicamarca LT = UT − 5.15. IMF = interplanetary magnetic field; ISR = incoherent scatter radar; C/NOFS = Communications and Navigation Outage Forecasting System; JULIA = Jicamarca Unattended Long-Term studies of the Ionosphere and Atmosphere.

were not covered during the process of developing the expression relating C/NOFS ion drifts and ΔH. Given that correlation coefficient values are above 0.75 in all cases with RMSE values comparable to some previous studies (e.g., Anderson et al., 2004) and even lower in some cases as is the case for the 13–15 November 2012 storm period (despite the limited data set available), we suggest that the developed relation can be utilized for all geophysical conditions. We restate that Anderson et al. (2004) obtained a RMSE value of 3.79 m/s using the same order of polynomial on ΔH and JULIA vertical drifts data during 2001–2003.

In detail, we present results for storm periods of 5–8 August 2011 and 8–10 March 2012 when ISR and JULIA observations were available, respectively. In both cases, we have compared our expression's performance with the earlier developed expression by Anderson et al. (2004). Figure 6 shows the observed (black dots) and derived $\mathbf{E}\times\mathbf{B}$ drift during the storm period of 5–8 August 2011. The derived vertical $\mathbf{E}\times\mathbf{B}$ drift velocities based on C/NOFS vertical $\mathbf{E}\times\mathbf{B}$ and ΔH expression are plotted as red dots. Corresponding values based on JULIA vertical $\mathbf{E}\times\mathbf{B}$ and ΔH relationship (expressed as $(\mathbf{E}\times\mathbf{B})_{A2004}$) from Anderson et al. (2004) are shown in blue dots. In the subsequent graphical representation where diurnal vertical $\mathbf{E}\times\mathbf{B}$ drift comparisons are performed, the colors of respective observed and derived vertical $\mathbf{E}\times\mathbf{B}$ drifts are similar to the description above. Shown in Figure 6a are the symmetric disturbance field in the *H* component, SYM-H (nT), and Bz component of the interplanetary magnetic field, IMF Bz (nT), in red and blue curves, respectively. The SYM-H index is equivalent to high-resolution *Dst* index (Wanliss & Showalter, 2006) and provides information about storm time ring current system. The occurrence of the 5 August 2011 geomagnetic storm was a result of complex changes in solar wind conditions that involved the launching of three coronal mass ejections on 2–3 August and became geoeffective on 4–5 August 2011 (Huang et al., 2014). On 6 August 2011 at 0322 UT, the SYM-H reached its peak value (−132 nT) of the main phase, and thereafter, the recovery process started and lasted at least 3 days. Figure 6 shows that at the commencement of the main phase onset (1906 UT or 1357 LT over Jicamarca on 5 August 2011), there was a sharp increase in vertical $\mathbf{E}\times\mathbf{B}$ drift (Figure 6b on 5 August 2011), which is a manifestation of penetrating electric field of magnetospheric origin (e.g.,Fejer & Scherliess, 1995, 1998; Huang et al., 2005) during the southward turning of IMF Bz and this was well reproduced by the developed mathematical expression (red dots). On 6 August 2011 during the recovery phase, the local daytime vertical drift decreased probably due to the westward electric field generated by the disturbed ionospheric dynamo

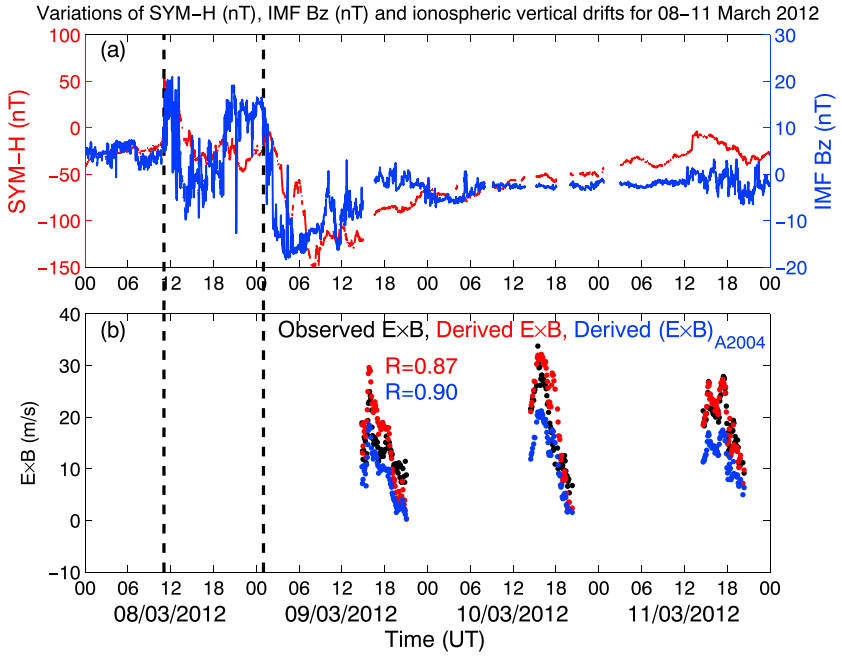

Figure 7. Variations in (a) SYM-H (nT) and IMF Bz (nT) for 8–11 March 2012 storm period, (b) JULIA observed (black dots) and derived vertical $\mathbf{E}\times\mathbf{B}$ (m/s) with C/NOFS (red dots) and JULIA (blue dots denoted as $(\mathbf{E}\times\mathbf{B})_{\mathbf{A2004}}$ obtained using expression developed by Anderson et al., 2004) based functions during the storm period of 8–11 March 2012. Vertical dashed lines correspond to the shock and main phase onset times at 1103 UT and 0100 UT on 8 and 9 March, respectively. IMF = interplanetary magnetic field; JULIA = Jicamarca Unattended Long-Term studies of the Ionosphere and Atmosphere; C/NOFS = Communications and Navigation Outage Forecasting System.

(e.g., Blanc & Richmond, 1980; Huang, 2013) and the dominance of *R*2 current when IMF Bz turns north (e.g., Kikuchi et al., 2000; Yizengaw et al., 2011). The developed expression not only follows the decreased vertical $\mathbf{E}\times\mathbf{B}$ velocities but also estimates well the magnitude of the vertical drifts. Overall, we obtained a high *R* value (0.92) between observed and derived vertical $\mathbf{E}\times\mathbf{B}$ drift velocities during the storm period of 5–8 August 2011. The computed RMSE of 4.37 m/s is less than the corresponding result (RMSE = 6.77 m/s) generated for the same order of polynomial in Anderson et al. (2004), which estimated vertical $\mathbf{E}\times\mathbf{B}$ velocities based on JULIA and ΔH measurements. The *R* value is similar (0.92) for both approaches during this storm period. What is significant is that our approach uses C/NOFS vertical $\mathbf{E}\times\mathbf{B}$ drift and ΔH observations and may be applicable even during geomagnetic storm conditions as shown in Figure 6b. Despite the differences in accuracy, the earlier developed relationship (Anderson et al., 2004) also follows the vertical $\mathbf{E}\times\mathbf{B}$ drift variability during this storm period. Figure 7 shows a comparison of JULIA observed and derived vertical $\mathbf{E}\times\mathbf{B}$ drift velocities for geomagnetically disturbed period of 8–10 March 2012. Figure 7a presents variations of SYM-H (nT) and IMF Bz (nT) plotted in red and blue colors, respectively. The vertical black dashed lines correspond to the times of the shock (1103 UT) and storm main phase onset (0100 UT) on 8 and 9 March 2011, respectively. The solar wind conditions and interplanetary causes of this storm period are detailed in Tsurutani et al. (2014). While the shock hit the Earth's magnetosphere at 1103 UT on 8 March, the storm main phase occurred on 9 March 2012 with SYM-H (nT) index reaching −148 nT at around 0800 UT. In Figure 7b, the observed (black dots) and derived (red and blue dots) vertical $\mathbf{E}\times\mathbf{B}$ drift velocities are compared during local daytime. Unfortunately, there were no JULIA vertical $\mathbf{E}\times\mathbf{B}$ drift observations as well as ΔH to derive $\mathbf{E}\times\mathbf{B}$ velocities on 8 March 2012. For the rest of the storm period, the variations in JULIA vertical $\mathbf{E}\times\mathbf{B}$ velocities are captured by the corresponding derived $\mathbf{E}\times\mathbf{B}$ drift velocities (red dots) with some occasional overestimation as is the case at around 1552 UT on 9 March during the sharp increase of the vertical $\mathbf{E}\times\mathbf{B}$ drift believed to be due to penetrating electric fields (Habarulema et al., 2016). Nevertheless, the derived vertical $\mathbf{E}\times\mathbf{B}$ drifts respond to the most important physical feature where penetrating electric fields of magnetospheric origin enhances the daytime eastward electric field in equatorial latitudes. For our approach based on C/NOFS vertical $\mathbf{E}\times\mathbf{B}$ and ΔH, the computed *R* and RMSE values are 0.87 and 4.31 m/s, respectively, during the 9–11 March 2012. The approach in Anderson et al. (2004) gives *R* and RMSE values of 0.90 and 6.67 m/s, respectively, and

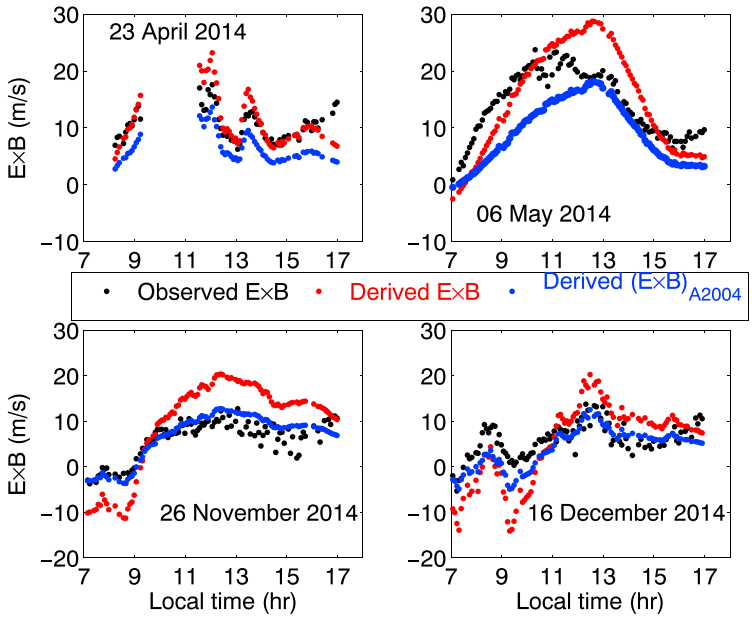

(a) ISR (black dots) and derived (red and blue dots) $\mathbf{E} \times \mathbf{B}$ (m/s) in 2014

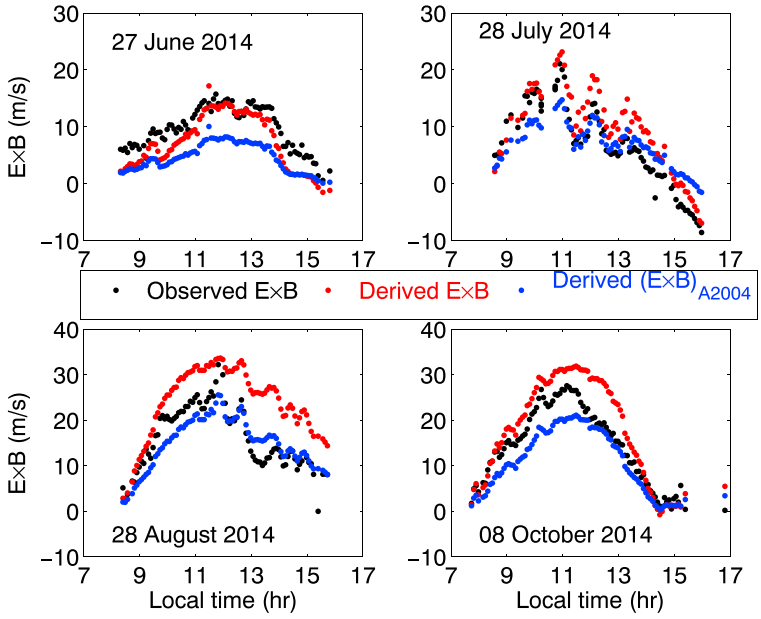

(b) JULIA (black dots) and derived (red and blue dots) $\mathbf{E} \times \mathbf{B}$ (m/s) in 2014

Figure 8. Comparison of observed ISR/JULIA (black dots) and derived vertical $\mathbf{E} \times \mathbf{B}$ (m/s) with C/NOFS (red dots) and JULIA (blue dots denoted as $(\mathbf{E} \times \mathbf{B})_{\mathbf{A2004}}$ obtained using expression developed by Anderson et al., 2004) based functions on randomly selected days in 2014 where measured data exist. (a) and (b) represent comparisons with ISR and JULIA measurements, respectively.

generally underestimates the observed vertical $\mathbf{E} \times \mathbf{B}$ drift velocities (see blue dots in Figure 7b). Generally, based on results in Figures 6 and 7 and Table 3, it is feasible to conclude that the developed expression based on C/NOFS vertical $\mathbf{E} \times \mathbf{B}$ drift and magnetometer ΔH observations is applicable in estimating vertical $\mathbf{E} \times \mathbf{B}$ velocities during geomagnetic storm conditions. Mathematically, this is possible and understandable as most of the daytime vertical drift changes are reflected in the EEJ (ΔH) measurements, which respond identically to vertical $\mathbf{E} \times \mathbf{B}$ drift during magnetically disturbed conditions. Finally, we validate our expression during other

Table 4
Correlation Coefficient (R) and Root-Mean-Square Error (RMSE) Values Computed Using Observed (ISR and JULIA) and Derived Vertical $\mathbf{E}\times\mathbf{B}$ *(m/s) for Some Days in 2014*

ISR with	C/NOFS(ΔH) func		JULIA(ΔH) func		JULIA with	C/NOFS(ΔH) func		JULIA(ΔH) func	
Date (2014)	*R*	RMSE (m/s)	*R*	RMSE (m/s)	Date (2014)	*R*	RMSE (m/s)	R	RMSE (m/s)
23 April	0.83	2.77	0.83	4.38	27 June	0.95	2.81	0.95	5.30
6 May	0.88	5.06	0.86	5.81	28 July	0.95	3.84	0.95	3.70
26 Nov	0.89	7.20	0.89	2.42	28 Aug	0.83	9.01	0.88	3.61
16 Dec	0.79	6.37	0.78	3.28	8 Dec	0.97	4.88	0.97	4.05

Note. Observed ISR and JULIA vertical $\mathbf{E}\times\mathbf{B}$ (m/s) are compared with corresponding vertical $\mathbf{E}\times\mathbf{B}$ (m/s) obtained using our expression based on C/NOFS vertical $\mathbf{E}\times\mathbf{B}$ (denoted as C/NOFS(ΔH) func) and Anderson et al. (2004) relationship (denoted as JULIA(ΔH) func), respectively. ISR = incoherent scatter radar; JULIA = Jicamarca Unattended Long-Term studies of the Ionosphere and Atmosphere; C/NOFS = Communications and Navigation Outage Forecasting System.

periods not covered by the data that were used to develop it. We recall that equation (1) was developed using C/NOFS vertical ion plasma drift (equivalent to $\mathbf{E}\times\mathbf{B}$) velocities and ΔH during the period of September 2008 to March 2014. Figure 8 shows observed and derived vertical $\mathbf{E}\times\mathbf{B}$ velocities on randomly chosen days within the period of May–December 2014 when ISR and JULIA made observations. Our approach is once again compared with derived vertical $\mathbf{E}\times\mathbf{B}$ drift velocities generated using expression in Anderson et al. (2004), which was developed based on JULIA and ΔH observations. Figure 8a graphically compares observed ISR (black dots) and derived (red and blue dots for our relationship and Anderson et al. (2004) expression, respectively) vertical $\mathbf{E}\times\mathbf{B}$ velocities for 23 April 2014, 6 May 2014, 26 November 2014, and 16 December 2014 during local daytime (0700–1700 UT). Figure 8b is similar to Figure 8a, but for JULIA and derived vertical $\mathbf{E}\times\mathbf{B}$ velocities on days 27 June 2014, 28 July 2014, 28 August 2014, and 8 October 2014. The statistical summary for the comparisons is presented in Table 4. In all cases, the *R* values computed from observed and our derived vertical $\mathbf{E}\times\mathbf{B}$ drift velocities are highly similar/comparable to the corresponding results when Anderson et al. (2004) expression is used. In terms of RMSE, with exception of 27 June 2014, the Anderson et al. (2004) expression gives lower values for observed JULIA vertical $\mathbf{E}\times\mathbf{B}$ drift comparisons. This is an expected result as Anderson et al. (2004) developed their expression based on JULIA vertical $\mathbf{E}\times\mathbf{B}$ drift and ΔH observations.

Figure 8 and Table 4 essentially demonstrate that it is possible to follow diurnal changes in vertical $\mathbf{E}\times\mathbf{B}$ drift velocities based on the polynomial function developed using C/NOFS vertical ion plasma drift and ΔH observations. This opens up new opportunities to develop low-latitude vertical $\mathbf{E}\times\mathbf{B}$ drift models using a combination of satellite and magnetometer measurements especially during local daytime that is accurate in all longitude sectors. In fact such models can be valid for all local times since satellites would also provide observations during nighttime (although sparse). Magnetometer measurements that are continuous and have high temporal resolution would then provide reliable daytime vertical $\mathbf{E}\times\mathbf{B}$ drift database. Pairs of magnetometers that satisfy the requirements to allow the development of expressions (similar to what has been done in this study) in different longitude sectors exist (e.g., Yizengaw et al., 2011, 2014) in African, American, Indian, and Asian sectors. Therefore, based on the presented results and approach, it is possible to develop new empirical vertical $\mathbf{E}\times\mathbf{B}$ drift models and update the existing ones such as the Scherliess-Fejer (SF) model (Scherliess & Fejer, 1999) and the ROCSAT-1 based quiet equatorial model (Fejer et al., 2008) to account for the recent unusual changes in solar activity such as the extended solar minimum of 2008–2010.

5. Conclusions

For the first time, a mathematical relationship between C/NOFS vertical ion plasma drift (equivalent to $\mathbf{E}\times\mathbf{B}$ drift at about 400 km) and magnetometer ΔH observations has been developed and validated with ISR and JULIA observations during local daytime (0700–1700 UT) covering a period of 2008–2014. While we restricted our analysis to Jicamarca (11.8°S, 77.2°W; 0.8°N geomagnetic) due to the availability of the actual observations to validate our approach, the order of the developed function is transferable to different longitude sectors, which have magnetometer locations that can estimate the EEJ. We stress that while the order of the polynomial can be kept, new coefficients should be derived for a different longitude sector to account for local contributions to vertical $\mathbf{E}\times\mathbf{B}$ velocities such as *E* region tides (both migrating and nonmigrating) influence on the electric field (Lühr et al., 2008; Maute et al., 2012; Millward et al., 2001). Overall, the developed expression can reconstruct at least 75% of the observed vertical $\mathbf{E}\times\mathbf{B}$ drift velocities from the ISR and JULIA observations. Of significant importance is the robustness of the polynomial function to also estimate vertical

$\mathbf{E} \times \mathbf{B}$ drift velocities during geomagnetic storms. Given the recent developments in magnetometer deployments to estimate the EEJ in different longitude sectors (Yizengaw et al., 2014), we suggest that the developed approach is a suitable basis for developing high-resolution empirical vertical $\mathbf{E} \times \mathbf{B}$ models even in longitudes without radar observations.

Acknowledgments
C/NOFS vertical $\mathbf{E} \times \mathbf{B}$ drift data were obtained from http://spdf.gsfc.nasa.gov/pub/data/cnofs/cindi/. The C/NOFS mission is supported by the Air Force Research Laboratory, the Department of Defense Space Test Program, the National Aeronautics and Space Administration (NASA), the Naval Research Laboratory, and the Aerospace Corporation. ISR and JULIA data were obtained from jro.igp.gob.pe. IMF Bz data are available from the Space Physics Data Facility website omniweb.gsfc.nasa.gov. The SYM-H index data were accessed from the World Data Center, Kyoto, Japan http://wdc.kugi.kyoto-u.ac.jp. This work is based on the research supported in part by the National Research Foundation of South Africa (grant 105778) and opinions, findings, and conclusions or recommendations expressed in this paper are of the author(s), and the NRF accepts no liability whatsoever in this regard. E. Y.'s work has been partially supported by AFOSR (FA9550-12-1-0437 and FA9550-15-1-0399) and NSF AGS145136 grants. M. B. M. was partially supported by the NSF grants AGS-1450512 and AGS-1654044.

References

Anderson, D., Anghel, A., Chau, J., & Veliz, O. (2004). Daytime vertical E× B drift velocities inferred from ground-based magnetometer observations at low latitudes. *Space Weather*, *2*, S11001. https://doi.org/10.1029/2004SW000095

Anderson, D., Anghel, A., Yumoto, K., Ishitsuka, M., & Kudeki, E. (2002). Estimating daytime vertical E × B drift velocities in the equatorial F-region using ground-based magnetometer observations. *Geophysical Research Letters*, *29*(12), 1596. https://doi.org/10.1029/2001GL014562

Blanc, M., & Richmond, A. D. (1980). The ionospheric disturbance dynamo. *Journal of Geophysical Research*, *85*, 1669–1686.

Chau, J. L., & Woodman, R. F. (2004). Daytime vertical and zonal velocities from 150-km echoes: Their relevance to F-region dynamics. *Geophysical Research Letters*, *31*, L17801. https://doi.org/10.1029/2004GL020800

Chen, Y., Liu, L., & Wan, W. (2011). Does the $F_{10.7}$ index correctly describe solar EUV flux during the deep solar minimum of 2007–2009?*Journal of Geophysical Research*, *116*, A04304. https://doi.org/10.1029/2010JA016301

Dubazane, M., Habarulema, J. B., & Uwamahoro, J. C. (2018). Modelling ionospheric vertical drifts over Africa low latitudes using empirical orthogonal functions and comparison with climatological model. *Advances in Space Research*, *61*, 326–336.

Ezquer, R. G., López, J. L., Scidá, L. A., Cabrera, M. A., Zolesi, B., Bianchi, C., et al. (2014). Behaviour of ionospheric magnitudes of F_2 region over Tucumán during a deep solar minimum and comparison with the IRI 2012 model predictions. *Journal of Atmospheric and Solar-Terrestrial Physics*, *107*, 89–98. https://doi.org/10.1016/j.jastp.2013.11.010

Fejer, B. G., de Paula, E. R., Gonzalez, S. A., & Woodman, R. F. (1991). Average vertical and zonal F region plasma drifts over Jicamarca. *Journal of Geophysical Research*, *96*(A8), 13,901–13,906.

Fejer, B. G., Jensen, J. W., & Su, S.-Y. (2008). Quiet time equatorial F region vertical plasma drift model derived from ROCSAT-1 observations. *Journal of Geophysical Research*, *113*, A05304. https://doi.org/10.1029/2007JA012801

Fejer, B. G., & Scherliess, L. (1995). Time dependent response of equatorial ionospheric electric field to magnetospheric disturbances. *Geophysical Research Letters*, *22*(7), 851–854.

Fejer, B. G., & Scherliess, L. (1998). Mid- and low-latitude prompt ionospheric zonal plasma drifts. *Geophysical Research Letters*, *25*(16), 3071–3074.

Habarulema, J. B., Katamzi, Z. T., Yizengaw, E., Yamazaki, Y., & Seemala, G. (2016). Simultaneous storm time equatorward and poleward large-scale TIDs on a global scale. *Geophysical Research Letters*, *43*, 6678–6686. https://doi.org/10.1002/2016GL069740

Huang, C. M. (2013). Disturbance dynamo electric fields in response to geomagnetic storms occuring at different universal times. *Journal of Geophysical Research: Space Physics*, *118*, 496–501. https://doi.org/10.1029/2012JA018118

Huang, C. M., Richmond, A. D., & Chen, M.-Q. (2005). Theoretical effects of geomagnetic activity on low-latitude electric fields. *Journal of Geophysical Research*, *110*, A05312. https://doi.org/10.1029/2004JA010994

Huang, C. Y., Su, Y.-J., Sutton, E. K., Weimer, D. R., & Davidson, R. L. (2014). Energy coupling during the August 2011 magnetic storm. *Journal of Geophysical Research: Space Physics*, *119*, 1219–1232. https://doi.org/10.1002/2013JA019297

Huber, P. (1981). *Robust statistics*. New York, USA: John Wiley & Sons.

Huber, P., & Ronchetti, E. M. (2009). *Robust statistics: Second edition*. New York, USA: John Wiley & Sons.

Hui, D., & Fejer, B. G. (2015). Daytime plasma drifts in the equatorial lower ionosphere. *Journal of Geophysical Research: Space Physics*, *120*, 9738–9747. https://doi.org/10.1002/2015JA021838

Kikuchi, T., Lühr, H., Schlegel, K., Tachihara, H., Shinohara, M., & Kitamura, T.-I. (2000). Penetration of auroral electric fields to the equator during a substorm. *Journal of Geophysical Research*, *105*(A10), 23,251–23,261.

Kudeki, E., & Fawcett, C. D. (1993). High resolution observations of 150 km echoes at Jicamarca. *Geophysical Research Letters*, *20*, 1987–1990. https://doi.org/10.1029/93GL01256

Kumar, S., Veenadhari, B., Tulasi Ram, S., Su, S.-Y., & Kikuchi, T. (2016). Possible relationship between the equatorial electrojet (EEJ) and daytime vertical E×B drift velocities in F region from ROCSAT observations. *Advances in Space Research*, *58*, 1168–1176. https://doi.org/10.1016/j.asr.2016.06.009

Leys, C., Ley, C., Klein, O., Bernard, P., & Licata, L. (2013). Detecting outliers: Do not use standard deviation around the mean, use absolute deviation around the median. *Journal of Experimental Social Psychology*, *49*(4), 764–766.

Lomidze, L., Knudsen, D. J., Burchill, J., Kouznetsov, A., & Buchert, S. C. (2018). Calibration and validation of swarm plasma densities and electron temperatures using ground-based radars and satellite radio-occultation measurements. *Radio Science*, *53*, 15–36. https://doi.org/10.1002/2017RS006415

Lühr, H., Rother, M., Häusler, K., Alken, P., & Maus, S. (2008). The influence of nonmigrating tides on the longitudinal variation of the equatorial electrojet. *Journal of Geophysical Research*, *113*, A08313. https://doi.org/10.1029/2008JA013064

Manoj, C., Lühr, H., Maus, S., & Nagarajan, N. (2006). Evidence for short spatial correlation lengths of the noontime equatorial electrojet inferred from a comparison of satellite and ground magnetic data. *Journal of Geophysical Research*, *111*, A11312. https://doi.org/10.1029/2006JA011855

Maute, A., Richmond, A. D., & Roble, R. G. (2012). Sources of low-latitude ionospheric E×B drifts and their variability. *Journal of Geophysical Research*, *117*, A06312. https://doi.org/10.1029/2011JA017502

Millward, G. H., Müller-Wodarg, I. C., Aylward, A. D., Fuller-Rowell, T. J., Richmond, A. D., & Moffett, R. J. (2001). An investigation into the influence of tidal forcing on F region equatorial vertical ion drift using a global ionosphere-thermosphere model with coupled electrodynamics. *Journal of Geophysical Research*, *106*(A11), 24,733–24,744.

Patra, A. K., Chaitanya, P. P., Mizutani, N., Otsuka, Y., Yokoyama, T., & Yamamoto, M. (2012). A comparative study of equatorial daytime vertical E×B drift in the Indian and Indonesian sectors based on 150 km echoes. *Journal of Geophysical Research*, *117*, A11312. https://doi.org/10.1029/2012JA018053

Patra, A. K., Chaitanya, P. P., Otsuka, Y., Yokoyama, T., Yamamoto, M., Stoneback, R. A., & Heelis, R. A. (2014). Vertical E×B drifts from radar and C/NOFS observations in the Indian and Indonesian sectors: Consistency of observations and model. *Journal of Geophysical Research: Space Physics*, *119*, 3777–3788. https://doi.org/10.1002/2013JA019732

Patra, A. K., & Rao, N. V. (2006). Radar observations of daytime 150 km echoes from outside the equatorial electrojet belt over Gadanki. *Geophysical Research Letters*, *33*, L03104. https://doi.org/10.1029/2005GL024564

Patra, A., Sripathi, S., & Tiwari, D. (2004). Coupling effect of the equatorial F region irregularities on the low latitude E region instability processes. *Geophysical Research Letters*, *31*, L17803. https://doi.org/10.1029/2004GL020486

Patra, A. K., Yokoyama, T., Otsuka, Y., & Yamamoto, M. (2008). Daytime 150 km echoes observed with the equatorial atmosphere radar in Indonesia: First results. *Geophysical Research Letters*, *119*, L06101. https://doi.org/10.1029/2007GL033130

Perna, L., & Pezzopane, M. (2016). foF2 vs solar indices for the Rome station: Looking for the best general relation which is able to describe the anomalous minimum between cycles 23 and 24. *Journal of Atmospheric and Solar-Terrestrial Physics*, *148*, 13–21. https://doi.org/10.1016/j.jastp.2016.08.003

Pingree, J. E., & Fejer, B. G. (1987). On the height variation of the equatorial F region vertical plasma drifts. *Journal of Geophysical Research*, *92*(A5), 4763–4766.

Rabiu, A. B., Folarin, O. O., Uozumi, T., Hamid, N. S. A., & Yoshikawa, A. (2017). Longitudinal variation of equatorial electrojet and the occurrence of its counter electrojet. *Annales Geophysicae*, *35*, 535–545. https://doi.org/10.5194/angeo-35-535-2017

Raghavarao, R., & Anandarao, B. G. (1980). Vertical winds as a plausible cause for equatorial counter electrojet. *Geophysical Research Letters*, *7*(5), 357–360.

Rastogi, R. G. (1974). Westward equatorial electrojet during daytime hours. *Journal of Geophysical Research*, *79*(10), 1503–1512.

Rastogi, R. G., & Klobuchar, J. A. (1990). Ionospheric electron content within the equatorial F2 layer anomaly belt. *Journal of Geophysical Research*, *95*(A11), 19,045–19,052.

Richmond, A. (1973). Equatorial electrojet—I. Development of a model including winds and instabilities. *Journal of Atmospheric and Terrestrial Physics*, *35*(6), 1083–1103. https://doi.org/10.1016/0021-9169(73)90007-X

Rodrigues, F. S., Smith, J. M., Milla, M., & Stoneback, R. A. (2015). Daytime ionospheric equatorial vertical drifts during the 2008–2009 extreme solar minimum. *Journal of Geophysical Research: Space Physics*, *120*, 1452–1459. https://doi.org/10.1002/2014JA020478

Rousseeuw, P., & Croux, C. (1993). Alternatives to the median absolute deviation. *Journal of the American Statistical Association*, *88*(424), 1273–1283.

Scherliess, L., & Fejer, B. G. (1997). Storm time dependence of equatorial disturbance dynamo zonal electric fields. *Journal of Geophysical Research*, *102*(A11), 24,037–24,046. https://doi.org/10.1029/97JA02165

Scherliess, L., & Fejer, B. G. (1999). Radar and satellite global equatorial F region vertical drift model. *Journal of Geophysical Research*, *104*(A4), 6829–6842. https://doi.org/10.1029/1999JA900025

Solomon, S., Qian, L., & Burns, A. G. (2013). The anomalous ionosphere between solar cycles 23 and 24. *Journal of Geophysical Research: Space Physics*, *118*, 6524–6535. https://doi.org/10.1002/jgra.50561

Stoneback, R. A., Davidson, R. L., & Heelis, R. L. (2012). Ion drift meter calibration and photoemission correction for the C/NOFS satellite. *Journal of Geophysical Research*, *117*, A08323. https://doi.org/10.1029/2012JA017636

Stoneback, R., Heelis, R., Burrell, A., Coley, W., Fejer, B. G., & Pacheco, E. (2011). Observations of quiet time vertical ion drift in the equatorial ionosphere during the solar minimum period of 2009. *Journal of Geophysical Research*, *116*, A12327. https://doi.org/10.1029/2011JA016712

Tsurutani, B. T., Echer, E., Shibata, K., Verkhoglyadova, O. P., Mannucci, A. J., Gonzalez, W. D., et al. (2014). The interplanetary causes of geomagnetic activity during the 7–17 March 2012 interval: A CAWSES II overview. *Journal of Space Weather and Space Climate*, *4*(A02), A02p1–A02p7. https://doi.org/10.1051/swsc/2013056

Vineeth, C., Pant, T. K., & Sridharan, R. (2009). Equatorial counter electrojets and polar stratospheric sudden warmings—A classical example of high latitude-low latitude coupling? *Annales de Geophysique*, *27*, 3147–3153.

Wanliss, J. A., & Showalter, K. M. (2006). High-resolution global storm index: *Dst* versus SYM-H. *Journal of Geophysical Research*, *111*, A02202. https://doi.org/10.1029/2005JA011034

Yizengaw, E., & Moldwin, M. B. (2009). African meridian B-field education and research (AMBER) array. *Earth, Moon, and Planets*, *104*(1-4), 237–246. https://doi.org/10.1007/s11038-008-9287-2

Yizengaw, E., Moldwin, M. B., Mebrahtu, A., Damtie, B., Zesta, E., Valladares, C. E., & Doherty, P. H. (2011). Comparison of storm time equatorial ionospheric electrodynamics in the African and American sectors. *Journal of Atmospheric and Solar-Terrestrial Physics*, *73*(1), 156–163.

Yizengaw, E., Moldwin, M. B., Zesta, E., Biouele, C. M., Damtie, B., Mebrahtu, A., et al. (2014). The longitudinal variability of equatorial electrojet and vertical drift velocity in the African and American sectors. *Annales de Geophysique*, *32*, 231–238.

Yizengaw, E., Zesta, E., Moldwin, M. B., Damtie, B., Mebrahtu, A., Valladares, C. E., & Pfaff, R. F. (2012). Longitudinal differences of ionospheric vertical density distribution and equatorial electrodynamics. *Journal of Geophysical Research*, *117*, A07312. https://doi.org/10.1029/2011JA017454